Planck pre-launch status: HFI ground calibration

F. Pajot, P.A.R. Ade, J.-L. Beney, E. Bréelle, D. Broszkiewicz, Philippe Camus, C. Carabétian, A. Catalano, A. Chardin, M. Charra, et al.

A&A 520, A10 (2010)
DOI: 10.1051/0004-6361/200913203

Astronomy & Astrophysics
Special feature

Pre-launch status of the Planck mission

Planck pre-launch status: HFI ground calibration

F. Pajot[1], P. A. R. Ade[2], J.-L. Beney[3], E. Bréelle[4], D. Broszkiewicz[4], P. Camus[5], C. Carabétian[1], A. Catalano[4], A. Chardin[1], M. Charra[1], J. Charra[1,†], R. Cizeron[3], F. Couchot[3], A. Coulais[6], B. P. Crill[7,8], K. Dassas[1], J. Daubin[3], P. de Bernardis[9], P. de Marcillac[1], J.-M. Delouis[10], F.-X. Désert[11], P. Duret[1], P. Eng[1], C. Evesque[1], J.-J. Fourmond[1], S. François[1], M. Giard[12], Y. Giraud-Héraud[4], L. Guglielmi[4], G. Guyot[1], J. Haissinski[3], S. Henrot-Versillé[3], V. Hervier[1], W. Holmes[8], W. C. Jones[8,13], J.-M. Lamarre[6], P. Lami[1], A. E. Lange[7,8,†], M. Lefebvre[1], B. Leriche[1], C. Leroy[1], J. Macias-Perez[14], T. Maciaszek[15], B. Maffei[16], A. Mahendran[1], B. Mansoux[3], C. Marty[12], S. Masi[9], C. Mercier[1], M.-A. Miville-Deschenes[1], L. Montier[12], C. Nicolas[1], F. Noviello[1], O. Perdereau[3], F. Piacentini[9], M. Piat[4], S. Plaszczynski[3], E. Pointecouteau[12], R. Pons[12], N. Ponthieu[1], J.-L. Puget[1], D. Rambaud[12], C. Renault[14], J.-C. Renault[10], C. Rioux[1], I. Ristorcelli[12], C. Rosset[3], G. Savini[17], R. Sudiwala[2], J.-P. Torre[1], M. Tristram[3], D. Vallée[4], M. Veneziani[4], and D. Yvon[18]

(Affiliations can be found after the references)

Received 28 August 2009 / Accepted 15 March 2010

ABSTRACT

Context. The *Planck* satellite was successfully launched on May 14th 2009. We have completed the pre-launch calibration measurements of the High Frequency Instrument (HFI) on board *Planck* and their processing.

Aims. We present the results ot the pre-launch calibration of HFI in which we have multiple objectives. First, we determine instrumental parameters that cannot be measured in-flight and predict parameters that can. Second, we take the opportunity to operate and understand the instrument under a wide range of anticipated operating conditions. Finally, we estimate the performance of the instrument built.

Methods. We obtained our pre-launch calibration results by characterising the component and subsystems, then by calibrating the focal plane at IAS (Orsay) in the Saturne simulator, and later from the tests at the satellite level carried out in the CSL (Liège) cryogenic vacuum chamber. We developed models to estimate the instrument pre-launch parameters when no measurement could be performed.

Results. We reliably measure the *Planck*-HFI instrument characteristics and behaviour, and determine the flight nominal setting of all parameters. The expected in-flight performance exceeds the requirements and is close or superior to the goal specifications.

Key words. cosmic microwave background – space vehicles: instruments – submillimeter: general

1. Introduction

The *Planck* satellite[1], launched on May 14th 2009, will map the sky in 9 frequency bands between 30 GHz and 1 THz. It is the third generation satellite dedicated to the study of the CMB (cosmic microwave background) after COBE and WMAP. Beeing the high frequency instrument on-board *Planck*, HFI covers frequencies between 100 and 857 GHz. The HFI receiver is based on cryogenic bolometric detectors operating at 0.1 K, a fraction of which are sensitive to polarisation. Pre-launch calibration is an essential step in characterising the instrument, estimating the sensitivity, optimising its operational parameters, and identifying its systematics. The calibration method of balloon-borne and orbital instruments in this frequency range is not well established. A diverse range of strategies have had to be devoped for different instruments and missions, such as COBE FIRAS (Fixsen et al. 1994), PRONAOS (Pajot et al. 2006), Archeops (Benoît et al. 2002), Boomerang (Masi et al. 2006), or WMAP (Page et al. 2003). This paper describes the method and results of the pre-launch calibration of the *Planck*-HFI at the instrument level. The *Planck* mission, the satellite, and its instruments are described in separate compagnion papers of this issue. In particular, the mission is detailed in Tauber (2010a), the LFI instrument in Bersanelli et al. (2010), and its ground calibration in Mennella et al. (2010).

The HFI instrument consists of 54 bolometers distributed between six frequencies of bandwidth $\Delta\nu/\nu = 1/3$, of which 32 are polarisation-sensitive bolometers (PSBs), 20 are unpolarized spider-web bolometers (SWBs), and two are dark bolometers monitoring common-mode systematics. The polarised detectors are oriented in the focal plane to enable the determination of the linear polarization using combinations of three or more channels. The detectors couple to the telescope by means of 36 back-to-back horn assemblies, including the optical filters defining the frequency bands. The bolometers, 16 thermometers on the 4 K, 1.6 K, and 100 mK thermal stages, a reference resistor, and a reference capacitor are read out by low noise electronics at the nominal acquisition rate (roughly 180 Hz). Four thermometers on the 4 K stage monitor the temperature of the HFI close to the location of the reference optical loads used by LFI. Other

[1] *Planck* (http://www.esa.int/Planck) is an ESA project with instruments provided by two scientific Consortia funded by ESA member states (in particular the lead countries: France and Italy) with contributions from NASA (USA), and telescope reflectors provided in collaboration between ESA and a scientific Consortium led and funded by Denmark.

Table 1. HFI design goals. P stands for polarisation sensitive bolometers.

Channel		100P	143P	143	217P	217	353P	353	545	857
Central frequency	(GHz)	100	143	143	217	217	353	353	545	857
Bandwidth	(%)	33%	33%	33%	33%	33%	33%	33%	33%	33%
Full width half maximum beam size	(′)	9.6	7.0	7.0	5.0	5.0	5.0	5.0	5.0	5.0
Number of bolometers		8	8	4	8	4	8	4	4	4
NE$\Delta T_{\rm CMB}$ per bolometer	(μK$_{\rm CMB}$ s$^{1/2}$)	100	82	62	132	91	404	277	2000	91 000
NE$\Delta T_{\rm R-J}$ per bolometer	(μK$_{\rm R-J}$ s$^{1/2}$)	77	50	38	45	31	34	23	14	9.4
Bolometer NEP	(aW s$^{1/2}$)	10.6	9.7	14.6	13.4	18.4	16.4	22.5	72.3	186

thermometers monitor the temperature of the 1.6 K and 4 K optical components, the 100 mK stage of the dilution cooler and the 100 mK bolometer plate. The 72 readout chains are distributed between twelve belts of six channels. Housekeeping telemetry includes all other thermometers and parameters sampled at longer intervals from one to several seconds. The cryogenic chain consists of passive cooling to 50 K achieved at the level of the third V-groove of the satellite, an 18 K hydrogen sorption cooler, a 4 K mechanical cooler based on compressed helium and a Joule-Thomson expansion, and a 100 mK dilution cooler. Table 1 summarises the optical and sensitivity goals of the *Planck*-HFI design. A complete description of the instrument is given in Lamarre et al. (2010).

The HFI calibration was carried out between September 2004 and August 2008 for two instrument models, the cryogenic qualification model (CQM) and the proto flight model (PFM). Each model of the focal plane unit (FPU), which consists of the receiver but not its 4 K cooling system, was tested in the Saturne cryostat of the calibration facility of the Institut d'Astrophysique Spatiale in Orsay, and on the satellite in the CSL (Centre Spatial de Liège) Focal 5 cryogenic chamber. The calibration philosophy is described in Sect. 2 and both the calibration setup and measurements in Saturne and in the CSL facility in Sects. 3 and 4 respectively. The results presented in Sect. 5 are intended to illustrate the measurements performed and reflect their quality. The calibration data used in the reduction process of the flight measurements are reported in the *HFI calibration and performance document* (Pajot et al. 2008) delivered to ESA and the scientific team, and in the IMO (instrument model), which is a numerical representation of calibration data used as an interface to the data processing pipeline.

2. *Planck*-HFI calibration strategy

2.1. Ground calibration goal

The goal of the pre-launch calibration is to provide

1. a final determination of parameters that cannot be measured in-flight;
2. a first estimate of parameters that can be measured in-flight;
3. an understanding of the instrument under a wide range of anticipated operating conditions;
4. an estimate of the in-flight instrument performance.

Figure 1 lists the parameters required when calibrating the flight data and the phases during which they have been or will be measured. The values determined for these parameters can be found in Sect. 5.

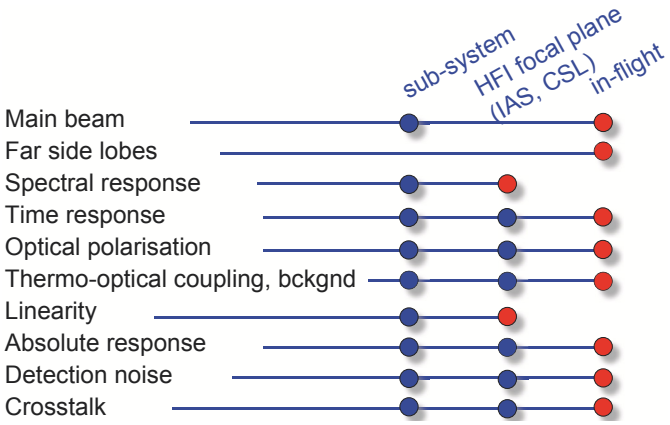

Fig. 1. Calibration philosophy. Blue dots indicate preliminary determinations, red dots indicate final determination.

2.2. Angular response

The angular response of the optical system includes the main beam and the far sidelobes and, at the sub-system level, the angular response of the feedhorn antenna of the bolometer assembly, the latter beeing measured for each feed. The preflight estimate of the beam (both the main beam and far sidelobes) is derived from both the measured feedhorn antenna pattern and either 1) the numerical simulation of the reflector system performed for the low frequency channels of HFI (Maffei et al. 2010) or 2) measurements performed on the RF (radio frequency) model of the telescope (Tauber et al. 2010b). This determination will be used until we are able to perform measurement for planets, which are measurements that are critical for studying the beam to 35-40 dB, and invert sky data for the far side lobes.

2.3. Spectral response

A measurement of the spectral response can only be performed on the ground. At the sub-system level, the spectral transmission of the filters and the horns were combined to predict the spectral transmission of each type of horn-filter assembly. The complete detector, filter, and horn assemblies, including the bolometric detector, were then measured in turn to determine the spectral response of each integrated pixel (Ade et al. 2010). Finally, the spectral response of the fully assembled focal plane was measured in the ground calibration facility. Ultimately, the spectral response is derived using both the measurements at the focal plane level and subsystem data to check or adjust for systematics. In a similar way, the efficiency of the out-of-band blocking was determined by a combination of individual measurements. It was also checked at the subsystem level by comparing the

response for sources with steep but with opposite spectral slopes (using high- or low-pass filters).

2.4. Time response

We measured the time response on the ground with signals modulated at frequencies covering the range 0.01 Hz to 100 Hz. Specific care was taken to measure the time transfer function at low frequency, since the absolute response for the low frequency channels (CMB channels) will be measured on the signal coming from the CMB dipole modulated by the spacecraft spin at ∼1/60 Hz.

The ultimate determination will be verified using the in-flight data by comparing the maps of the same bright sources, such as planets, obtained with different scan directions and angles at different phases of the mission.

2.5. Optical polarisation

The absolute orientation of the polarisation and the cross-polar leakage are deduced from both the sub-system measurements and the FPU characterisation. Polarisation orientation and cross-polar leakage are measured on individual horn assemblies and the absolute orientation of the FPU is measured by taking into account the geometry of the beam (Rosset et al. 2010).

The pre-launch determination of the beams and polarisation parameters was achieved using measurements of the FPU (Maffei et al. 2010) and the radio frequency (RF) model of the telescope (Tauber et al. 2010b).

The polarised emission of the Crab nebula was measured at the IRAM 30 m telescope at frequencies near the HFI bands. These data are used to derive the final calibration of the sky data (Aumont et al. 2010). The galaxy polarisation is poorly known today and is not neglible. At low frequencies measurements do exist (Archeops, Benoît et al. 2002). New observations at short wavelengths (e.g., PILOT balloon experiment, Bernard et al. 2007) will be used to improve our understanding of the polarised emission on the sky at these frequencies.

2.6. Optical efficiency, linearity, and sensitivity to the temperature of the cryogenic stages

This group of parameters characterises the instrument behaviour over an extended range of operational conditions. The optical efficiency is the fraction of photons collected by the real optical system with respect to an ideal system of same spectral response. Bolometric detectors have a linear response when the optical signal is weak relative to the optical background, but a determination of the linearity curve is needed for photometric calibration at the percent level. In addition, knowledge of the dependence of the signal on the temperature fluctuations of all optical components is essential to reduce the thermal systematic effects. The instrument thermal design includes very stable thermal regulation systems that are designed to keep these effects below the detector noise (see Sect. 5.3.2). The characterisation of the coupling coefficients gives, if required, the possibility of removing second order correlations of thermal origin between channels. These parameters are measured at the level of the detector subsystems, during the focal plane calibration, and are confirmed with in-flight measurements.

2.7. Absolute calibration

The absolute calibration allows one to convert the digital signal into the sky brightness. The HFI does not use any internal absolute reference signal, therefore the total power is not reliably measured by the HFI bolometers. The full sky maps deduced from the HFI data are instead insensitive to a constant emision level, such as the CMB monopole. A preliminary absolute response was estimated during the focal plane calibration with a precision of 10% (and a relative pixel to pixel calibration of 3%). The ground calibration sources allowed us to perform this measurement with an optical background that was representative of that expected in-flight. The final determination will be performed in-flight (Piat et al. 2002). The goal is a 1% radiometric accuracy for the low frequency channels ($\nu < 400$ GHz: 100, 143, 217, 353 GHz) and 3% for the high frequency channels ($\nu > 400$ GHz: 545, 857 GHz). The FIRAS experiment on the COBE satellite has provided the most accurate photometric calibration for extended sources in the millimeter and submillimeter wavelength range producing a spectral image of the sky in the range [0.1, 10 mm] (3000 GHz to 30 GHz), with a spectral resolution of approximately 5% and a spatial resolution of 7°. FIRAS used an absolute black body to provide a flux calibration with an accuracy superior to 1% below 400 GHz and 3% above (Mather et al. 1999). The in-flight calibration of the submillimeter channels of HFI will rely on this calibration. The CMB dipole component, produced by the proper motion of *Planck* with respect to the rest frame of the CMB, will be used for the low frequency channels. Therefore, the absolute calibration procedures can be detailed as follows:

1. For the channels below 353 GHz, the CMB dipole dominates the galactic signal over most of the sky. The observed dipole is the sum of two components, one resulting from the peculiar velocity of the solar system in the CMB rest frame, another resulting from the orbit of the Earth, hence the L2 point and *Planck*, around the Sun. As long as the circles described on the sky have a different axis from that of the dipole (the angle is always larger than 10°, which provides more than 15% of the dipole signal), a short-term relative calibration can be obtained from the dipole: the relative variation in the dipole signal is at most 0.9% per day or 4×10^{-2}% per hour, i.e., between two consecutive depointings. This allows a straightforward ring to ring relative calibration limited only by the level of the CMB fluctuations. The use of WMAP data could improve the ring calibration, although the absolute calibration will be obtained in a self consistent way from the orbital dipole, observed on the survey timescale (6 months), more accurately than 0.4% (Piat et al. 2002).
2. For the channels above 353 GHz, Galactic emission is the dominant component. The Galactic signal has a high spatial frequency component that makes relative calibrations from ring to ring impossible because rings have a large angular separation (2 arcmin, about half of the FWHM beam of these channels). Observations of the Galactic disk at submillimeter wavelengths exist only at lower angular resolution (typically 30 arcmin with balloon observations) with absolute calibrations that are poorer than 10 to 20%, and at the very low spatial resolution of FIRAS with an absolute calibration of 3% above 400 GHz. We will average HFI data over one week periods and more to obtain a pixel size of 7° identical to that of FIRAS. This requires knowledge of the temporal variation in the relative response over this timescale without the benefit of an external calibration source. An instrument model

based on the thermometry and the ground calibration will be used to provide a relative calibration of the sub-millimeter channels on the scale of a week. Future balloon experiments observing the galactic structure in the submillimeter range on angular scales comparable to HFI *Planck* (e.g., PILOT) will also provide valuable information about this relative calibration. Finally, the absolute calibration of FIRAS will be used to obtain the required 3% accuracy.

2.8. Detection noise

Although noise in the detectors and in the readout electronics can potentially have a significant impact on the ultimate sensitivity of the measurements, the goal of the HFI is to reach the ultimate physical limitation which is the intrinsic statistical fluctuations in the astrophysical background and foreground photons. The detector noise was measured during all phases of the instrument development starting with the electrical NEP of *blind* bolometers, and continuing with an optical background equivalent to the expected flight background on the integrated horn, filter, and bolometer subsystems. These measurements were also reproduced during the focal plane calibration. The detector noise measurements were carried out across a wide range of frequencies, from a few mHz to the cut-off frequency of the low pass filter needed by the analog-to-digital conversion of the lock-in detection (a few kHz). The DPU (digital processing unit) can provide the full sampling of any pixel before demodulation. This DPU operation mode was used to monitor and measure the noise level at audio frequencies during the FPU ground calibration and in-flight. However the most important measurements will come from in-flight data obtained in the demodulated (nominal) mode of the DPU. The ground-based measurements will be used to understand these data and to extract the different contributions to this noise including background photon noise, intrinsic detector noise, voltage and current noise in the electronics, and the temperature stability of both the optical components and the detectors.

2.9. Crosstalk

During the focal plane calibration, the electrical crosstalk was checked by applying a bias signal to each bolometer in turn and monitoring the response of the neighboring devices. To simulate the stray capacitance of the wiring on the spacecraft, a harness identical to the flight harness was used for the ground test setup. On the ground, optical crosstalk and spectral leaks were checked at the FPU level using illuminators in front of a subset of the pixels. In-flight limits to the crosstalk amplitude will be deduced from the sky data by applying two methods:

- scans across bright point sources, including planets;
- measurements of the cross-correlation between channels.

2.10. Readout electronics

The characteristics of the readout electronics are measured at both the subsystem level (without the bolometers) and the instrument level. The bolometers are bias modulated at a frequency close in value to 180 Hz. The bias frequency is derived from a clock common to the 4 K cooler compressors which is operated exactly at 1/4.5 times this frequency, or about 40 Hz. The 4 K cooler is the only mechanical subsystem operated above the spin frequency of the satellite (1 rpm). The stability of the bias generator, the pre-amplifier and amplifier gains, and the readout electronic noise are continuously monitored during the flight. The bias control parameters were optimised both during the focal plane calibration and in-flight for the actual instrument and telescope background prior to the initiation of the first survey. Absolute in-flight calibration requires that the response of the instrument be stable or at least well known for periods of at least 15 days (see Sect. 2.7). The absolute calibration of the measurement chain does not need to be superior to a few percent, although knowledge of the relative response must be accurate to a fraction of a percent, with a goal of 0.2% accuracy for the relative time response and deviation from linearity. A similar accuracy is required for the change of response with the background (static load on bolometers) and bolometer plate temperature. These accuracies are achieved by performing dedicated calibration tests, both on the ground and during the flight, and by using sophisticated models of the detection chain.

2.11. Compatibility

All compatibility issues are checked on the ground. Tests are carried out at the FPU level and during the tests of the integrated satellite: compatibility with the cryocoolers, with the LFI, and with the service module subsystems. The susceptibility of the detectors and electronics to high energy particles hitting was monitored during the focal plane calibration. Based on the prelaunch knowledge of the particle environment at L2 and depending on the energy threshold, the rate of particle hits at L2 is expected to be between 1 and 10 hits per minute. For these rates, and based on the amplitude of the particle hits observed on the signal during the calibrations, masking the data to below the level of the noise removes a negligible fraction of the integration time. However, the true rate and the corresponding energy will be known only in orbit.

3. Focal plane calibration in the Saturne cryostat

The focal plane of HFI was calibrated in the Saturne cryostat of the calibration facility of the Institut d'Astrophysique Spatiale in Orsay. The HFI focal plane consists of the detectors, the optical filters and horns, the 100 mK stage of the dilution cooler, and the thermo-mechanical structure and its interfaces with the 4 K and 18 K cryocoolers. We designed and built an optical and cryogenic simulator dedicated to this calibration.

3.1. Description of the Saturne simulator for HFI

3.1.1. Optical layout

The main difficulty in performing calibration measurements of the HFI is simulating a radiative background environment that is representative of the L2 orbit. An additional complication is the repeatable simulation of the very low amplitude signal expected from the astrophysical sources (Fig. 2). To achieve these requirements, the Saturne cryostat gives a thermal environment consisting of a 2 K enclosure that contains the HFI FPU and the optical calibration system. The calibrator is an integrating sphere fed by both internal sources and a path to external sources. A spherical mirror couples the output of the calibrating sphere to the FPU. Finally, an instrumented wheel can be deployed in front of the FPU, producing polarization and optical crosstalk measurements (Figs. 3 and 4). The 2 K enclosure (Fig. 5) is optically sealed, and the optical bench is partially covered by Thomas Keating microwave absorber so that the cavity behaves like a 2 K blackbody source when all other sources are either turned

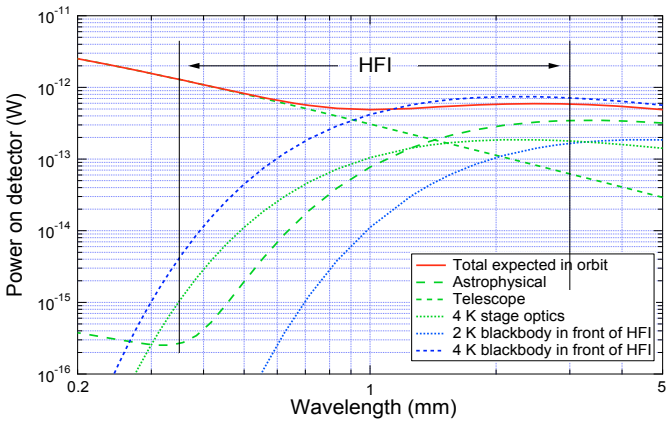

Fig. 2. Background radiation absorbed by the single mode detectors (λ^2 etendue) with a $\Delta\lambda = \lambda/4$ bandwidth. The telescope emission is simulated by a 60 K *Planck* spectrum with an emissivity of $0.005(\lambda/1\ \mathrm{mm})^{-1/2}$.

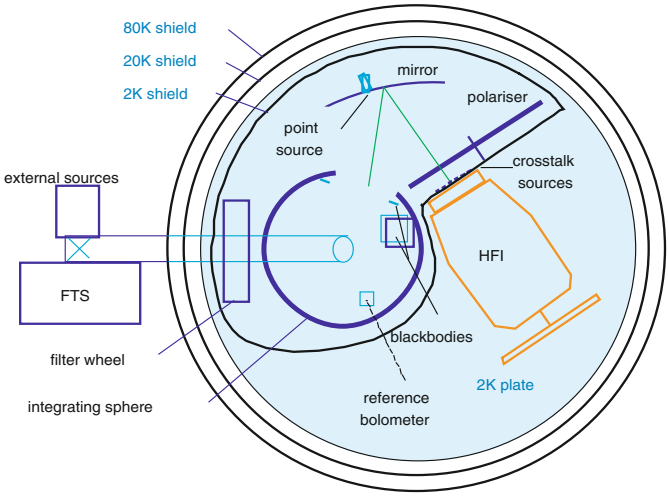

Fig. 3. Optical diagram of the HFI FPU calibration setup in the Saturne cryostat.

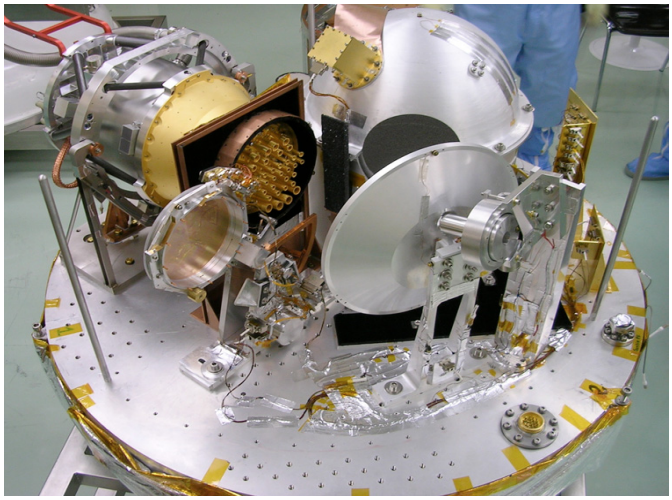

Fig. 4. Optical setup on the 2 K Saturne cryoplate with the HFI PFM. The polariser and sources on the instrumented wheel are positioned out of the optical path to the integrating sphere.

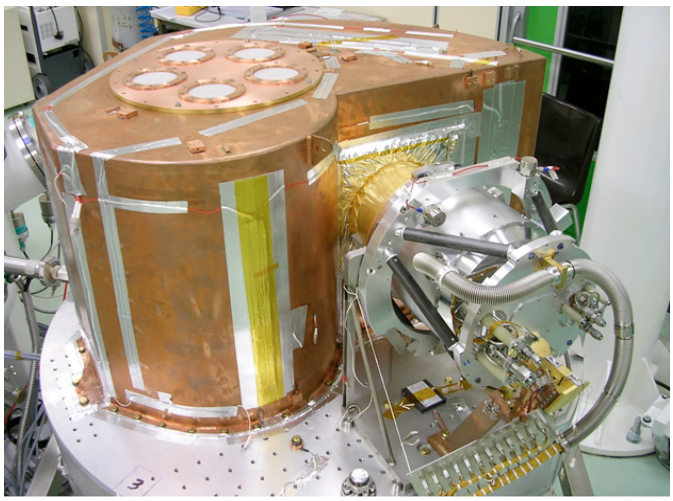

Fig. 5. Optical setup after integration of the 2 K optical baffle. The HFI detectors are looking into the 2 K enclosure. Only the back of the HFI PFM is visible, with its 4 K and 18 K interfaces.

off or blocked. The 2 K cavity is itself enclosed by vapor-cooled 20 K and 80 K shields. The scattering of the light inside the sphere is obtained by a pseudo random machining of its inner surface. Two internal thermal sources and two external sources (an external chopped source and a Fourier transform spectrometer) feed the integrating sphere.

3.1.2. The Saturne cryostat

The Saturne cryostat (Fig. 6) was used to perform the ISOCAM calibrations (Vigroux et al. 1993). However, we completed an important redesign to meet the requirements for the ground calibration of the HFI instrument. The Saturne cryostat consists of a vacuum chamber (1600 mm high, 1604 mm diameter) attached to the ground by three legs. All the utilities and all the hermetic interfaces are located at the bottom of the vacuum chamber. The HFI calibration requires 24 h periods of operation that are uninterrupted by cryogen transfers from the 4 K storage tank to the 2 K chamber. The lowest temperature achieved is 1.8 K.

3.1.3. HFI thermal interfaces

The HFI FPU provides only the 100 mK dilution cooler stage. The Saturne cryostat provides the cooling interfaces simulating:

- the 50 K stage for the cold JFET preamplifier box (the JFET themselves are heated to 130 K);
- the 18 K sorption cooler;
- the 4 K Joule-Thomson cooler;
- the LFI.

3.1.4. Internal optical sources

The integrating sphere is fed by two low-power thermal sources:

1. CS1 is an emissive ring heated to a temperature adjustable to 30 K, with an effective etendue of 1000 mm^2 sr, located inside the integrating sphere. This black body produces a background similar to that expected from the *Planck* telescope in flight conditions.

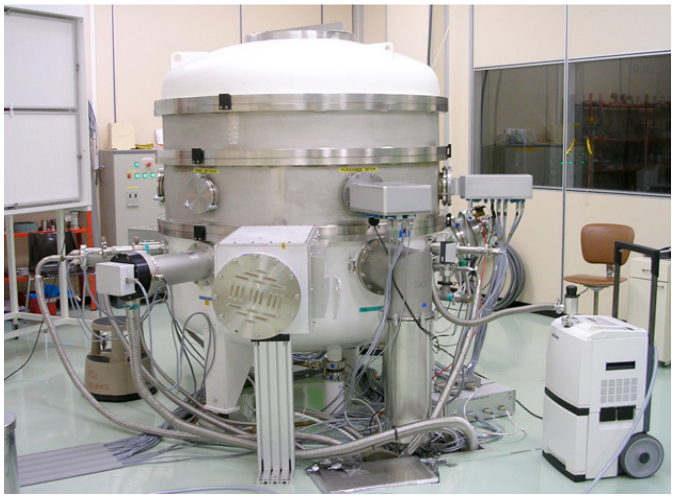

Fig. 6. The Saturne cryostat in the class 10 000 clean room. The two upper rings and the lid are removable for the integration of the calibration optics and the instrument. The optical port is on the opposite side.

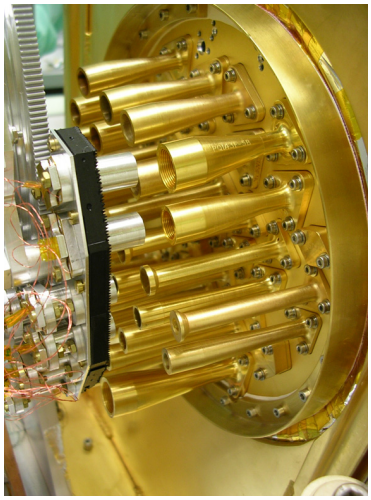

Fig. 7. Carbon fiber sources (OXT) in place in front of the HFI horns.

2. CS2 is a black body heated to a temperature adjustable to 20 K, and modulated at a fixed frequency close to 10 Hz by means of a resonant tuning fork chopper.

Two other sources provide signals with a short time constant. These sources are based on carbon fibers self-heated by Joule dissipation of the electrical current (Henrot-Versillé et al. 2009). Their optical flux is collimated by horns:

1. CSM is a carbon fiber located in a horn that couples directly to the focal plane through a hole inside the mirror. It illuminates all pixels simultaneously.
2. OXT refers to a set of carbon fiber sources located on the instrumented wheel that can be positioned in front of a subset of the HFI pixels. The coupling is sufficiently directional for only the corresponding pixels to be illuminated, allowing a measurement of the optical crosstalk at the per mil level (Fig. 7).

3.1.5. External optical sources

The polarising Fourier-transform spectrometer (FTS) was provided by Sciencetech Inc. (Canada) under contract with IAS and

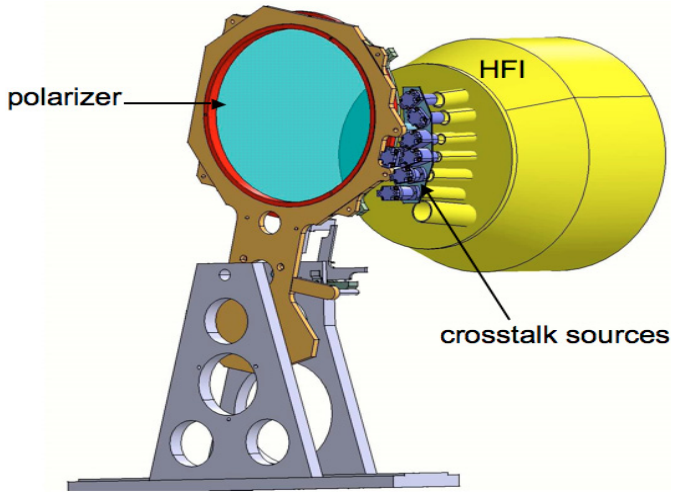

Fig. 8. The three-position instrumented wheel that supports the rotating polariser and the crosstalk sources.

ESA. It is derived from the SPS200 model. The source can be selected from either a Mercury vapour arc lamp or a Globar (a silicon carbide rod heated by the Joule effect). The 300 mm translation stage generates symmetric interferograms with a maximum theoretical (unapodized) resolution of 0.035 cm^{-1}. Filtering of short wavelengths in the optical path entering the Saturne cryostat is achieved using:

- a vacuum window made of polyethylene (6 mm thick);
- a 1st thermal filter at 300 K;
- a 2nd thermal filter at 77 K;
- a 46 cm^{-1} cut-off filter at 77 K;
- a 3rd thermal filter at 20 K;
- a filter wheel at 2 K allowing the selection between four configurations of open, closed, 35 cm^{-1}, and 10 cm^{-1} cut-off filters.

While scanning, encoder pulses from the translation stage are time stamped with a clock that is synchronized with the HFI signal acquisition clock (provided by the spacecraft simulator used during the calibration). In a similar way, a mechanical zero path difference (ZPD) signal is stamped and stored in the database. After verification, we found that the scanning speed was sufficiently stable to be considered as constant along the section of the interferogram needed for spectral processing. To provide a reference monitor for the source flux, a dedicated bolometer was used within the integrating sphere. The flux received by this reference bolometer is directly proportional to the flux received by the HFI pixels on the focal plane, which is coupled via a mirror to the integrating sphere output aperture. The reference bolometer was provided with an absolute calibration by the team of N. Coron and J. Leblanc at IAS. It is fed by a modified Winston horn from Infrared Lab. Inc. (USA) and operated at 300 mK using a ^{3}He fridge (Torre & Chanin 1985). The reference spectra acquired during the calibration run with this bolometer were used to identify standing wave features in the FTS source and optical path (lamp, windows, ...) and to check the shape of the source spectrum. The diffraction losses at low frequencies due to the horn exit aperture diameter (2.6 mm) are taken into account in the data processing of the low frequency channels of HFI. The FTS signal is fed into the Saturn cryostat and the integrating sphere through a vacuum pipe by means of collimating mirrors. An alternate path through this pipe allows the use of either a mercury arc lamp or a Globar chopped by a 300 K

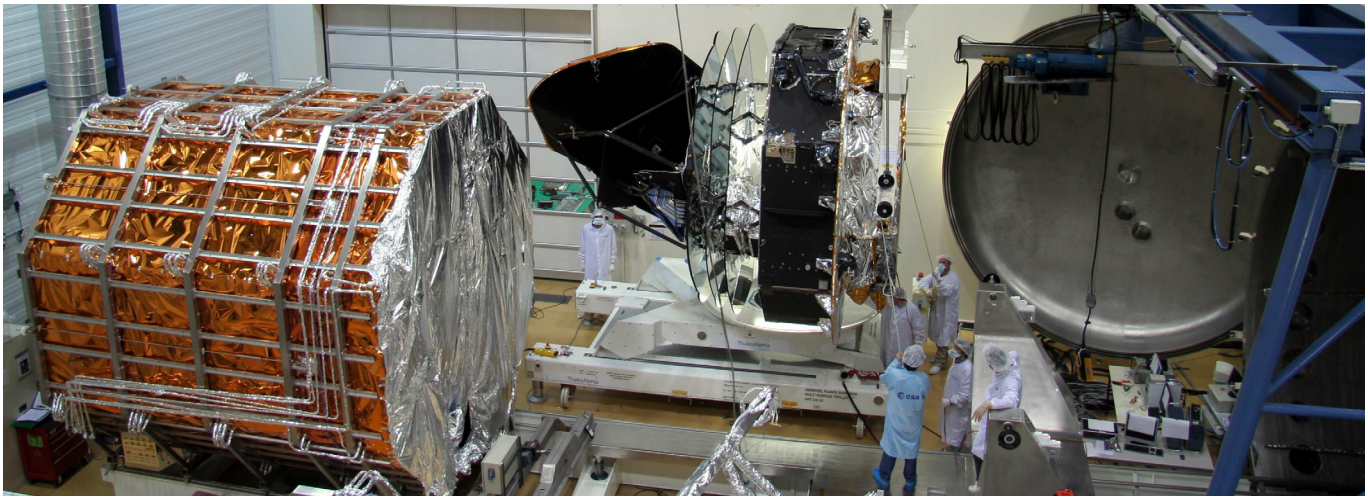

Fig. 9. *Planck* in configuration ready to enter into the CSL Focal 5 cryogenic simulator.

rotative blade, operated at ambient temperature in vacuum conditions. Chopping this source allows the measurement of the time response of the HFI to 1 ms rise time signals, down to 1 Hz.

3.1.6. Polarisers

The instrumented wheel (Fig. 8) moves a rotating polariser directly in front of the HFI feed horns. A detailed description of the setup and the measurement method of the polarisation properties of HFI can be found in Rosset et al. (2010).

3.2. Measurement campaigns

Two measurement campaigns of the HFI PFM were carried out in Orsay in 2006: the characterisation in March (4 days of scientific measurements with the HFI dilution cryocooler at an operational temperature close to 100 mK, 28 days for the total duration of the campaign including cooldown and warmup), and the calibration in June–July (20 days and 42 days, respectively).

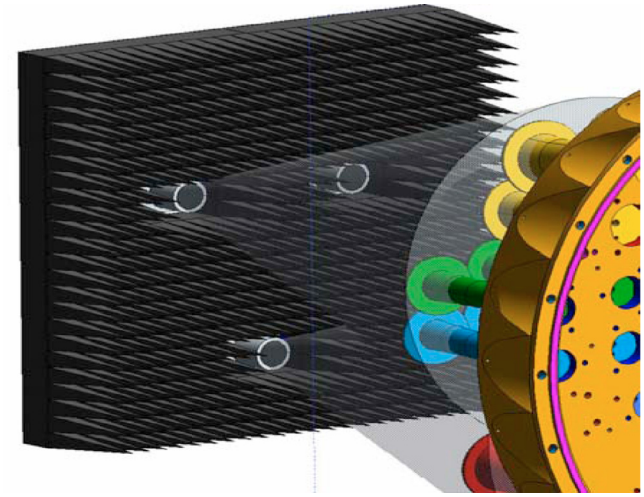

Fig. 10. Skyload: panel of Eccosorb pyramids cooled at 4 K, within which 3 carbon fiber sources are located with their collimating horn.

4. CSL TV-TB characterisations

4.1. The test optical configuration

From the point of view of the HFI, the goal of the thermal vacuum – thermal balance (TV-TB) testing was the validation of the cryogenic chain including the 4 K cooler operation and the end-to-end test of the detection chain with cold detectors (auto-compatibility and compatibility with both LFI and the spacecraft). Following the measurements in the Saturne cryostat, a more accurate characterisation of the low frequency time response of the bolometers was also performed during the CSL PFM campaign. The optical setup was the following:

- the satellite was in the Focal 5 cryogenic simulator of CSL (Fig. 9).
- the complete cryogenic chain (passive cooling, 18 K and 4 K cryocoolers, 100 mK dilution) was operated.
- a skyload was placed just in front of HFI and LFI horns, in front of the secondary mirror. The skyload is an Eccosorb panel cooled to 4 K by liquid helium, equipped with three sensitive thermometers (carbon glass type from LakeShore Inc.). Three carbon fiber sources (similar to the OXT sources) are placed at the center of the skyload during the PFM campaign to illuminate the HFI focal plane (Fig. 10). The sources can be biased with an arbitrary waveform.

4.2. Measurements and results

The CQM TV-TB campaign was held from June to September 2005. It allowed us to partially characterise the cooling chain and check compatibility issues. The total duration of the PFM TV-TB campaign was 3 months (mid-May to mid-August 2008) and the HFI detectors were cold (around 100 mK) for 15 days. The active cooling chain performed nominally, with an overall performance that exceeded the requirements. The detection chain and bolometer functional tests exhibited very good self and mutual compatibility.

The behaviour of all HFI detectors was identical to that in the Saturne cryostat: all 52 (non-*blind*) bolometers detected the background fluctuations (Fig. 11). The I-V characteristics of the bolometers agree with previous measurements (a finely sampled network of curves at various bath temperatures in Fig. 12). Bolometer NEPs (1 to 3 $\times$ 10^{-17} $\mathrm{WHz}^{-1/2}$) are similar to the values obtained during the calibration campaign in the Saturne

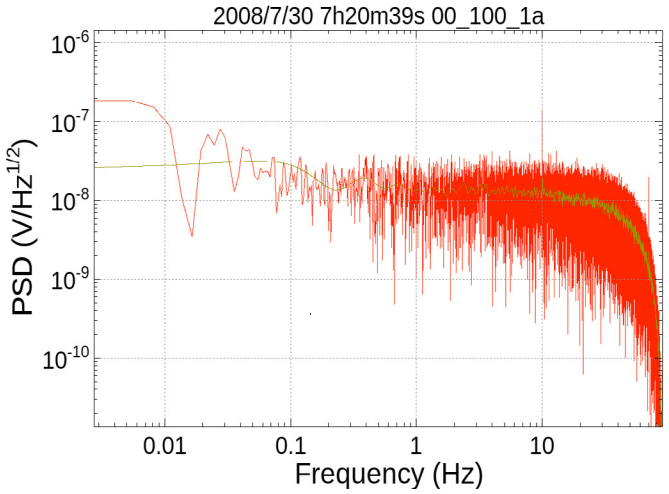

Fig. 11. Amplitude spectral density of the signal of an HFI channel, during the TV-TB tests. The cut-off observed at high frequency results from the numerical filtering of the signal. The rise at low frequency is due to the thermal fluctuations of the skyload and the thermal environment in the Focal 5 simulator. The bolometer represented is the 100 GHz channel number 00-100-1a.

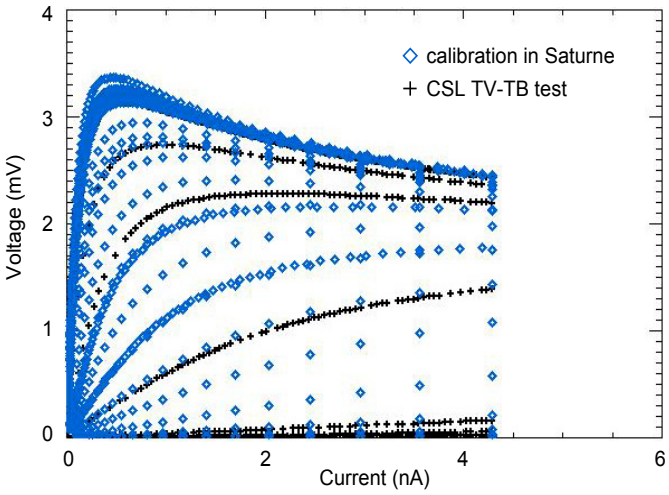

Fig. 12. Network of I-V characteristics for various temperatures of the bolometer plate and background, during the Saturne calibrations and the TV-TB tests. The bolometer represented here is the 100 GHz channel number 00-100-1a.

cryostat. Given the superior control of the background environment in the Saturne cryostat, pre-launch sensitivities are derived from the Saturne measurement.

Popcorn noise (2-level oscillation at random intervals ranging from a fraction to several seconds), already seen in the Saturne cryostat, was observed on only two detectors during the TV-TB campaign. Glitch rates and time constants are similar to those seen in the PFM focal plane calibration in Saturne. When the LFI was switched off, changes in the HFI noise level were smaller than 1%. During the simulated DTCP (daily telecommunication period), the transponders were activated as they would for the communications to the Earth over periods of 3 to 6 h integration. The noise spectra differed by less than 2.5% peak. No noticeable influence from either LFI or the transponder could be detected.

5. Calibration and performance outline

We now present the main results of the *Planck-HFI calibration and performance document* (Pajot et al. 2008) delivered to ESA and which will be the reference for the flight data processing by the scientific team. Only global results are discussed here because we aim to demonstrate the validity of the method and the conformity of the instrument with the requirements.

5.1. Optics

5.1.1. Beam geometry

The coupling of the bolometers to the telescope is provided by the FPU optics consisting of an assembly of filters, lenses, and horns. The beam pattern of the single mode channels depends to first order only on the 4 K front horn, since the propagating wave is defined in the single mode waveguide section of the back-to-back horn. The spectral and geometrical properties of the horns have been characterised individually. The measured beam pattern of a typical front horn is compared with the prediction made at the design stage. The agreement is excellent to very low levels (% level), which supports our following characterisation of the horns (Maffei et al. 2002):

- modelling and optimizing the horns before implementation;
- validating the model on some prototypes with a complete measurement of the beam patterns (intensity and phase);
- checking the beam pattern intensity of all the horns and relying on the fit to derive the phase.

The beam patterns of all single mode front horns were measured. The most accurate estimate of the amplitude and phase of these horns were used for the pre-launch beam estimation (Maffei et al. 2010). The beam patterns of the multi-moded channels depend on all optical elements within the entire optical path. Beam predictions of the multimoded channels are less accurate than for the single-moded channels. To achieve a more reliable assessment, a campaign of dedicated measurements on spare multi-moded channels with an improved experimental set-up has been performed at Cardiff University.

Most of the photons selected by the horns arrive from the telescope's mirrors, which intercept a solid angle of about 27 degrees half-angle. The spillover can be defined as the overall radiative power reaching the detector that does not originate from the telescope's reflector. This results in a signal that does not originate in the observed source, and is therefore an important parameter in assessing straylight and far-side lobe control. Predictions and measurements of the far-side lobes were made on the RFQM (radio frequency qualification model) and modeled in addition using GRASP 9 (Tauber et al. 2010b).

To estimate the beam on the sky, we computed the propagation from the bolometers to the sky using the most reliably validated models of the various optical elements. The complete scheme relies on mechanical and RF measurements at the component and sub-system level, on the validation of modelling tools, on tests at the system level (RFQM, RFFM), and on flight data (Tauber et al. 2010b).

5.1.2. Spectral transmission

The in-band Saturne measurements show a noise floor of 10^{-2} to 10^{-3}. The distribution of the 3 dB cut-on, central, and 3 dB cut-off frequencies shows a good match of all pixels within the same band, but with some slight differences (Fig. 13) between

Table 2. HFI optical efficiencies assuming top-hat like channel spectral transmissions with nominal bandwidth edges.

Channel		100P	143P	143	217P	217	353P	353	545	857
Average efficiency	(%)	32.2	43.2	28.7	31.3	25.7	21.3	23.4	15.7	13.1
Dispersion	(1σ, %)	4.1	3.55	1.5	2.7	1.1	2.8	5.8	1.4	2.2

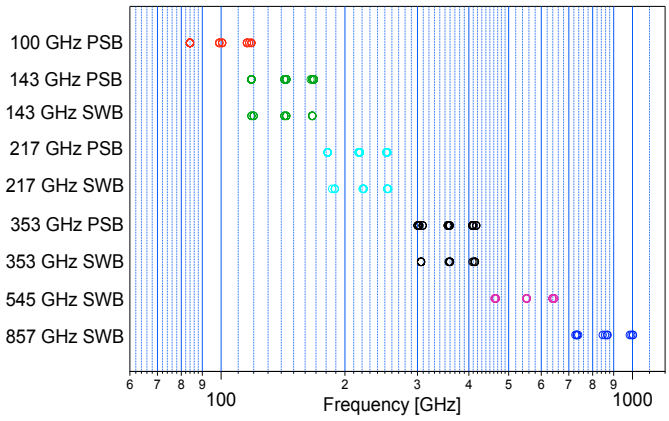

Fig. 13. 3 dB cut-on, central and 3 dB cut-off frequencies of all detectors of all HFI bands.

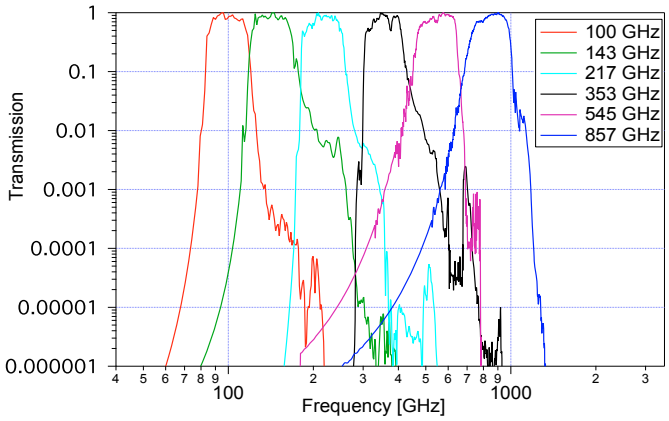

Fig. 14. Averaged normalized HFI spectral bands compiled using Saturne measurements (above 1%) and component characterisations (below 1%).

PSB and SWB channels. The rejection of lower frequencies can be obtained from waveguide theory with a good level of confidence. However, for the multi-moded channels, the transmission between the waveguide cut-on and the high-pass filter cut-on can be conservatively estimated to be the product of the transmission of the single optical components as measured. Rejection of higher frequencies is computed from the product of the single filter transmission data. Each set of data has a noise floor of about 10^{-3} so that the combined information can reach a level of 10^{-15}. The blocking of high frequencies was checked at the pixel subsystem level, and the FPU calibration data agree with these. An example of the resulting spectral bands is shown in Fig. 14. Detailed information can be found in Ade et al. (2010).

5.1.3. Total optical efficiency

The most straightforward definition of the optical efficiency is the ratio of the power detected by the bolometer through its optics, to the power that would be observed with perfectly transmitting optical elements in-band and complete rejection out-of-band. The measurement of the end to end optical efficiency is needed to estimate its absolute calibration and deduce the expected sensitivity of the instrument. The measurement was performed by varying the temperature of the 2 K optical platform from 2 K to 3.7 K, while regulating all thermal stages of HFI at constant temperature. Table 2 shows the efficiencies obtained from the ground calibration (Maffei et al. 2010). The absolute calibration will be obtained from observations of the sky during the flight.

5.1.4. Spectral dependence of beams

For convenience, the spectral transmission and the beam shape are often considered to be independent quantities. In reality, the beam pattern on the sky depends on the product of the spectral intensity of the source and the shape of the transmission of each channel. This dependence was studied for both single mode and multimoded channels in Maffei et al. (2010).

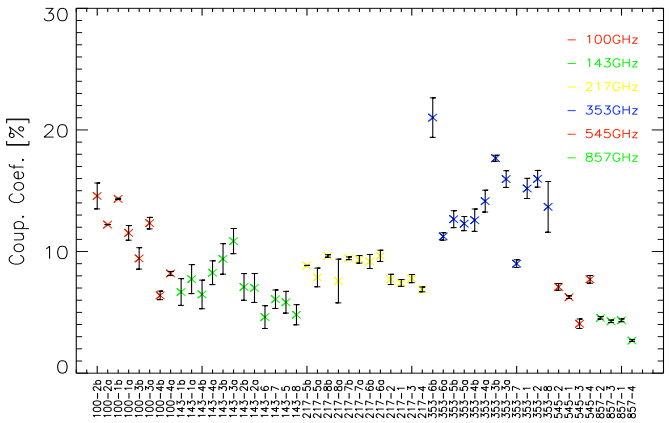

Fig. 15. Coupling coefficients of the 4 K stage. The error bars represent the statistical errors deduced from repeated measurements in different conditions.

5.1.5. Emissivity of the 4 K and the 1.6 K stages of the FPU

The thermal emission of the optical components on the 4 K and 1.6 K stages of the FPU is part of the optical background power absorbed by the bolometers. The thermal regulation of these stages are designed to limit the level of the fluctuations seen by the detectors below the noise of the detection chain. The optical coupling of these stages with the detectors was measured in the Saturne cryostat (Figs. 15 and 16).

5.1.6. Optical crosstalk

While illuminating one pixel by the OXT source in place, an upper relative value of 10^{-3} was measured for the signal coming from a non-illuminated pixel. The crosstalk signals generated by the only pixels facing an OXT source were checked. This value agrees with the expected flux diffracted from the OXT sources.

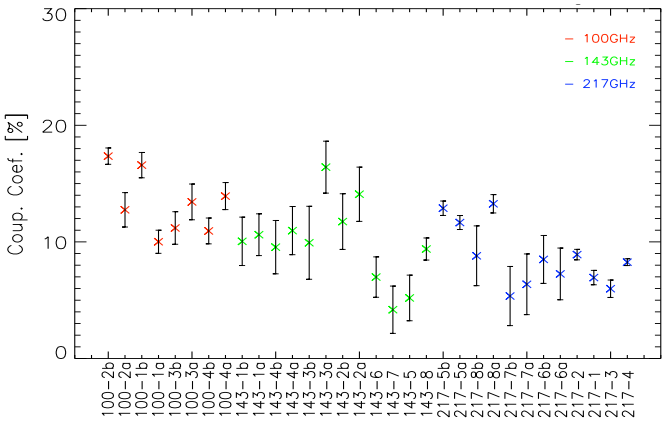

Fig. 16. Coupling coefficients of the 1.6 K stage. These coefficients could be measured only for the low frequency channels, the thermal emission in high frequency bands being too small to be measured. The error bars represent the statistical error deduced from repeated measurements in different conditions.

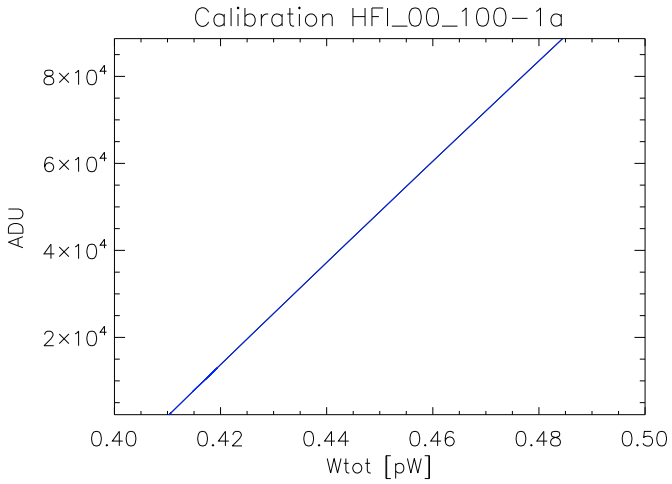

Fig. 17. Response function of the instrument for the 00-100-1a bolometer.

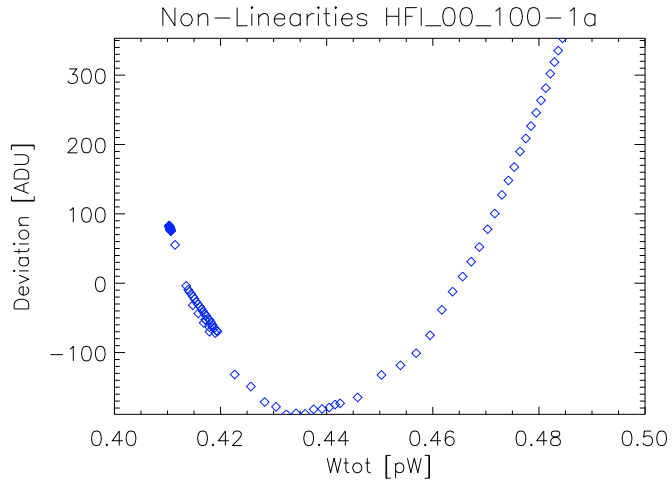

Fig. 18. Deviation from a linear response for channel 00-100-1a. The channel deviation from linearity in this range of background is smaller than 1%.

5.1.7. Polarisation specific parameters

Cross-polar leakage is measured at the level of individual pixel assemblies. The results show a typical value for the cross-polarisation leakage of PSB of 5%, ranging from 2 to 9%. The errors in these parameters is very low, below 0.2% (absolute error) except for one PSB for which it is 1.3%. The SWB are also minimally sensitive to polarisation, with cross-polarisation leakage ranging from 84% to 97%, and errors typically about 0.5%, except 3% for one SWB.

The axes of polarisation sensitivity are measured in the Saturne cryostat. The distribution of errors in angle measurement is 0.6° for PSB and 5° for SWB. A detailed analysis and results are presented in Rosset et al. (2010).

5.2. Response of the detection chains

5.2.1. Static response

The AC biasing of the HFI detectors allows one to perform a total power measurement. The static response function is the relation between the incoming power (in Watts) and the instrument output data (in digital units or ADU), once all transients have vanished. It is expected to be non-linear because both the thermal conductance between the bolometer and the heat sink, and the bolometer impedance have a non-linear dependance with temperature (Holmes et al. 2003). The static response function was measured during the PFM ground calibration in the Saturne cryostat under a wide range of background conditions. The local derivative of this response function infers the responsivity, which is the quantity that will ultimately be derived from the in-flight calibration on the sky (see Sect. 2.7). During the ground tests, the responsivity is measured by illuminating all bolometers by the CSM carbon fibre source modulated at a frequency of about 1 Hz. The average background power is explored by slowly changing the temperature of the CS1 source. Results are presented in Fig. 17 for a 100 GHz bolometer. The non-linearity of the detector is the deviation of this instrument function with respect to a linear one as shown in Fig. 18. Results show that the HFI bolometers are linear up to relative deviations of the order of 0.1% (Saturne planet at 353 GHz). Saturation of the read-out electronics is expected on bright sources for some channels. If we overplot the expected output for the second brightest source for HFI, the Saturn planet, we can observe that the saturation of the electronics appears only for the highest frequency channels (Fig. 19). The central lobe of the main beams will therefore not be deduced from in-flight measurements of Jupiter or Saturn, but fainter sources such as Mars or Uranus (Huffenberger et al. 2010).

5.2.2. Temporal response

The temporal response function or transfer function of the HFI detection chain results from both the bolometer intrinsic thermal time response and the coupling of the readout electronic chain to the detector. The former results from the complex thermal architecture of SWB and PSB, the latter from the presence of stray capacitance in the detection chain. The accuracy goal of the characterisation of the time response of the instrument is an accuracy superior to 0.2% within the [10 mHz, 70 Hz] range. For a subset of the bolometers, the analysis of the ground calibration data clearly detects an enhanced response at low frequencies. This low frequency excess response (LFER) concerns the range of frequencies lower than a few Hz. Thus, the time response function can be described as a cut-off filter function with at least 2 time constants and weights. A very accurate knowledge of the HFI response at these low frequencies is a key point for

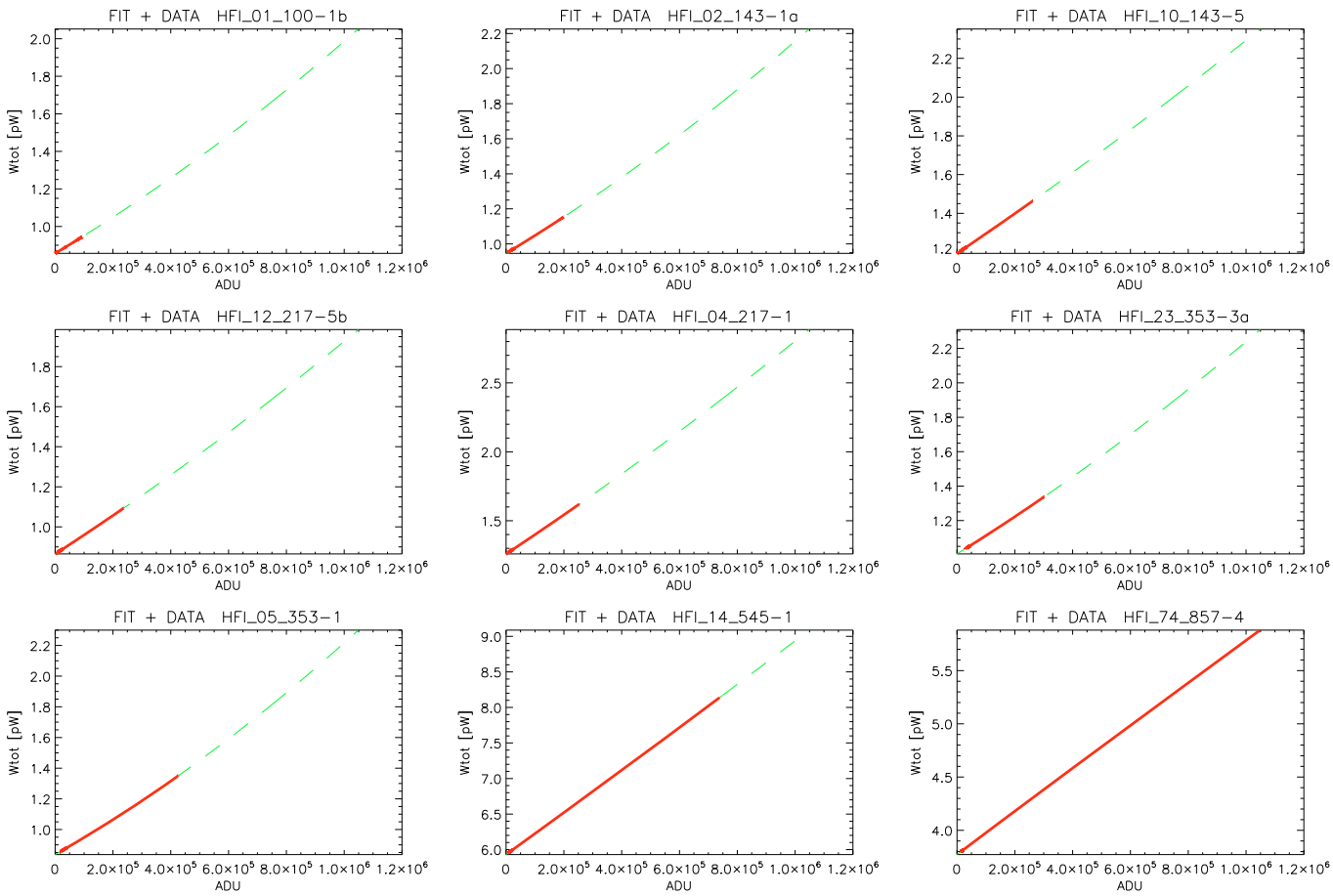

Fig. 19. Extrapolation of the response up to saturation. The range covered by Saturn is overplotted (solid red line).

scientific goals because, for most of the channels, the calibration of HFI is obtained by a measurement of the CMB dipole signal that appears in *Planck* at the frequency of 16.7 mHz. The following measurements are performed to characterise the time response:

- The time response from 2 to 100 Hz is measured with the chopped external source (ELS sequence).
- the low frequency range of the time response (from 8 mHz to 10 Hz) is measured with a carbon fiber source to produce a square modulation of period equal to up to 120 s. This measurement is valid only in the low frequency range because the intrinsic time response of the carbon fiber source is not negligible with respect to the bolometer time constant. Unfortunately, the setup used for this measurement done during the CSL TV-TB test (see Sect. 4), did not properly illuminate 20 of the 52 pixels of HFI.
- an additional measurement that does not rely on any external source was performed to determine the transfer function in the low frequency range. The bolometer is excited by a step in its bias current, which dissipates an additional electrical power in the bolometer. This sequence can be reproduced in-flight. However, the computation of the time response from a bias step measurement is more complex than that required from an optical illumination measurement because the physical processes involved differ. A representative determination of the time response function is shown in Fig. 20.

The temporal response functions for all bolometers were measured during the CSL TV-TB test using at least one of these two methods. An excess in the bolometer response below a few Hz has been identified. The amplitude of the excess response ranges from 0.1% to a few percent (Lamarre et al. 2010). Improving the knowledge of these functions in the low frequency range is still necessary for 20 (of 52) bolometers that could not be characterised more accurately than 0.5% during the CSL campaign. In addition to these approaches, simulations were performed to complete the time response functions using the in-flight data themselves. For this purpose, we will use measurements taken at various times of the survey with different scan directions.

5.2.3. Numerical compression

The data flow from the detectors (i.e., the science data) need to be compressed to conform to the telemetry rate allocated to HFI (75 kbit/s). The lossy quantization performed by the DPU adds some extra noise to the data. Given a flat probability error distribution within $[-Q/2, Q/2]$, where Q is the quantization step, the total power after quantization of a white Gaussian noise of standard deviation σ is expected to be

$$\sigma_{\rm tot} \approx \sigma \sqrt{1 + \frac{(Q/\sigma)^2}{12}} \,. \quad (1)$$

For a properly balanced detector with $\sigma/Q = 2$, this adds 1% to the level of the noise. This was checked using simulations and

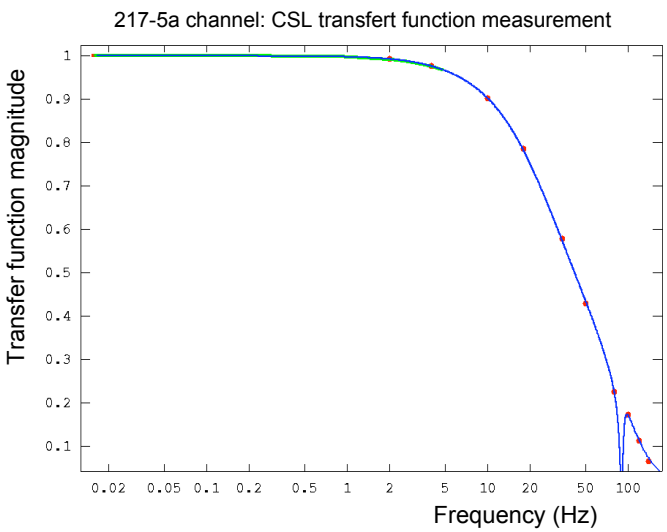

Fig. 20. HFI time response from 10 mHz to 120 Hz for the 11-217-5a bolometer. These results concern two different sequences. The green curve results from the bias current step sequence. The red points result from the ELS sequence. The blue curve is the empirical model deduced from the analysis.

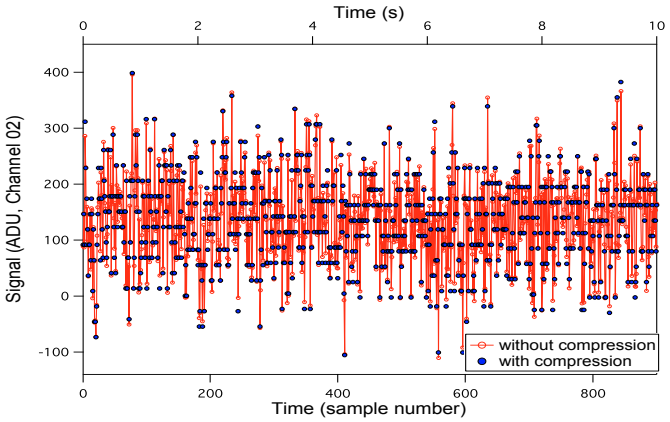

Fig. 21. Demodulated signal obtained with and without numerical compression. The 02-143-1a bolometer is shown. The quantization step used is ≈1/2 times the standard deviation. The compression is performed per slice of ≈1.4 s duration.

during ground tests using a dedicated mode of the DPU allowing the transmission of both the uncompressed and compressed data from the detectors (Fig. 21). The compression settings on non-CMB channels is less stringent than that on CMB channels: compression settings planned for the flight take into account both the telemetry allocation bandpass and the end-to-end simulations carried out to check the impact on the science result.

5.2.4. Electrical crosstalk

The electrical crosstalk is the effect of the signal of a pixel or of a thermometer coupling electrically into the signal of another pixel or thermometer. It takes two forms:

– When the bias current of a detector is changed, a capacitive coupling might affect the signal of another detector. This will in turn change its response. The parasitic signal induced in this case is not correlated with the signal of the modified detector. This effect is the *current crosstalk*.

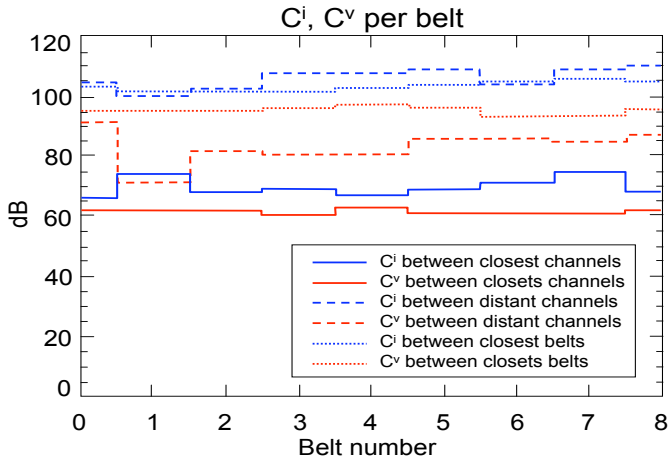

Fig. 22. Electrical crosstalk measured for the PFM during the Saturn calibrations. HFI detectors are organized in 12 belts of 6 detectors each.

– When all detectors are polarised with a fixed (modulated) current, the response remains constant but electromagnetic interference along the signal path generates a signal in another pixel that is in phase with the first. This effect is the *voltage crosstalk*.

Detailed measurements have been carried out at subsystem level with the FET box and, during the Saturne and CSL PFM tests, at instrument level. The electrical crosstalk was measured with a dedicated telecommand sequence consisting of switching off the bias current one detector at a time, without using any optical source. The results (Fig. 22) show coupling factors lower than 60 dB for neighbouring channels and lower than 80 dB for distant channels. This meets the requirements (60 dB) for all channels. The *voltage crosstalk* at constant bias current was also measured during the Saturne PFM calibration by sending a strong modulated optical signal when the CSM source is in the focal plane, biasing only one detector and looking for a correlated signal on a *blind* detector located in the focal plane. This directly infers the voltage crosstalk signal for a given pair of detectors. An upper limit of 60 dB was found, with an average of 90 dB, in agreement with the previous method.

5.2.5. Noise analysis

Understanding the noise behavior is of utmost importance to the cosmological analysis. The different noise components that are expected and/or measured in the HFI detectors are listed here:

– The dominant part of the noise is nearly white and Gaussian. This is true for all detectors. Figure 23 shows an example of the power spectrum of four bolometers during quiet conditions and under the expected flight background. The Gaussian part of the noise dominates the spectrum from 0.1 Hz to the modulation frequency of 86 Hz. At a mean level of about 20 nV/sqrt(Hz), it constists mostly of photon noise, phonon noise, Johnson noise (a typical 10 MOhm impedance will produce 7.4 nV/sqrt(Hz) at 100 mK), and 6 nV/sqrt(Hz) of the electronics (JFET). The measure of the noise within a resistor in the focal plane using the same readout as the bolometers is in agreement with expectations. The noise was studied as a function of bias current, JFET temperature, and base plate temperature. All detectors record valid signals and are dominated by Gaussian noise. Figure 24 compares the corresponding sensitivities with the goal values

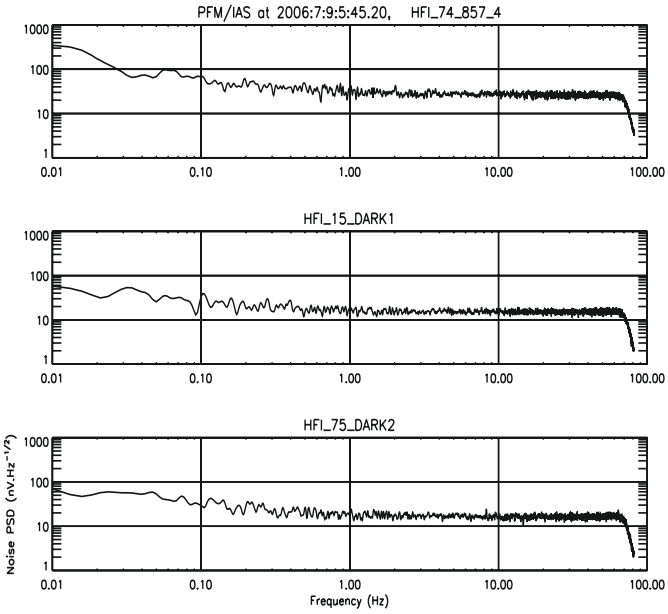

Fig. 23. Noise power spectrum of three bolometers during the Saturne calibrations: the 74-857-4, the dark 1 and the dark 2. The noise spectral density is shown from 10 mHz to 100 Hz, just above the modulation frequency. The high frequency drop is due to the post-processing filtering. The low frequency noise is slightly above the white noise because of some 0.1 K fluctuations (for the dark bolometers) and some Saturne background fluctuations (for the 857 GHz bolometer).

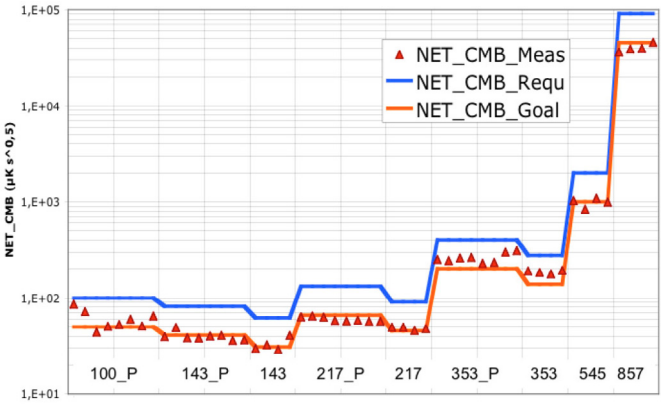

Fig. 24. Individual sensitivity of all bolometers measured during calibrations compared to requirement and goal. The goal is twice as high as the requirement. Sensitivities are consistent with the overall mission goals given in the *Planck* Blue Book (The *Planck* consortium 2005).

(Table 1). A detailed discussion of sensitivities can be found in Lamarre et al. (2010).

- During the ground tests, the PFM bolometers receive particle impacts at a rate varying from 1 to 20 per hour, depending on the bolometer.
- Because of the AC modulation scheme of the bolometers, we do not expect $1/f$ noise from the electronics. Using the 10 MOhm resistor channel, we see that this is indeed the case for frequencies above 3 mHz. For bolometers, signals caused by fluctuations in both the background and the base plate temperature mimic $1/f$ noise. This set an upper limit to the noise because a stable enough state could not be reached during the ground-based tests.
- Some of the HFI photometric pixels are affected by popcorn or telegraphic noise. The signal hops from one value to another as if in a two-level system. During the CSL campaign, the instrument being integrated in the satellite, only two channels exhibiting strong telegraph noise were identified (70-143-8 and 55-545-3), while many channels were during the HFI PFM calibration in Orsay.
- Under vibrations, the detector signal can contains microphonic lines at some specific frequencies. During the PFM tests in Saturn and at CSL, excitation was produced and found to originate in the facilities themselves (Helium refill, cryocoolers, etc.). The only lines identified as originating in the satellite and instrument were due to the 4 K active cryocooler of HFI. However, these lines were dominated by EMI/EMC interferences known to originate from the drive electronics of this cooler. These lines are very narrow because both the data acquisition rate and the cooler frequency are determined by a common clock. They are removed from the time domain data using a moving average template. The microphonic contribution is very weak, and cancelled when the vibration control system (VCS) of the 4 K cooler is activated. Therefore, the frequency of the 4 K cryocooler used during the CSL ground tests will be used during the flight.

5.3. Thermal behaviour

5.3.1. Static performance of the cooler and operation point

The behaviour of the full HFI cryogenic chain could not be tested in the Saturne test cryostat because the sorption cooler and the 4 K cooler are integrated in a complex way in the spacecraft and the payload module. They all rely on the passive cooling provided by the 3rd V-groove and the warm radiator, which radiates into deep space the power of the sorption cooler. Tests and qualification were carried out at the sub-system level or with an incomplete setup for the CSL CQM tests, until the CSL PFM campaign began. The overall performance of the cryogenic chain were derived from this latter campaign.

The performance of the 4 K cooler concerns

- the heat lift capability;
- the temperature of the cold head providing the pre-cooling of the gases of the dilution cooler;

as a function of the adjustable parameters

- the compressors frequency;
- the stroke amplitude;

and the environment parameters

- the pre-cooling of the helium gas by the sorption cooler;
- the temperature of the base plate of the compressors.

The filling pressure was chosen to be 4.5 bars. The lowest resonance frequency of the spacecraft panel on which the compressors are mounted is 72 Hz. We therefore chose a frequency above 37 Hz. The operating frequency affects the efficiency of the cooler (ratio of heat lift to electrical power). This efficiency shows a broad maximum around 40 Hz. Furthermore, because of the failures of the lead-in wires and the change of design, the risk are minimized by selecting a frequency lower than 45 Hz. We thus chose a frequency in the possible range between 37.41 and 41.74 Hz and preferably one of the three frequencies used during the TV-TB tests (37.41, 40.08, and 41.74 Hz). In view of a limited and well understood EMI-EMC and microphonics lines seen in the data (mostly generated by the CSL facility), our choice of the nominal frequency is 40.08 Hz. Furthermore, the frequency

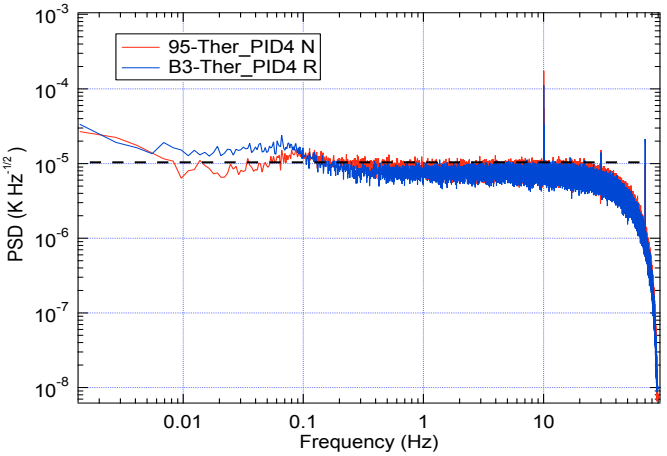

Fig. 25. 4 K stage temperature power spectrum during the CSL TV-TB campaign. The active PID is controlled by the thermometer 95-Ther PID4 N. The dashed line shows the requirement.

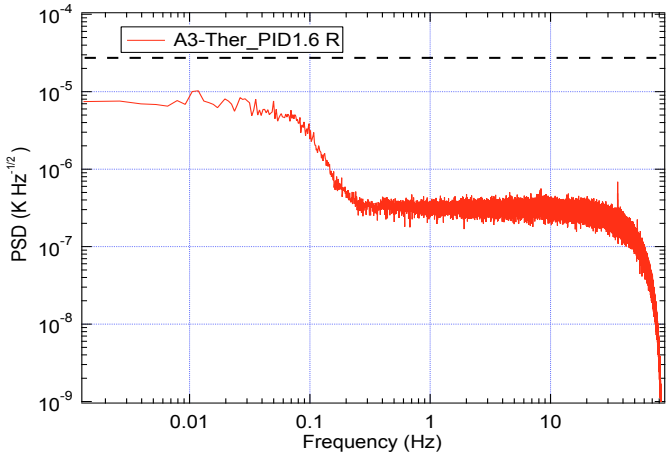

Fig. 26. 1.6 K stage temperature power spectrum during the Saturne PFM calibration. The dashed line shows the requirement.

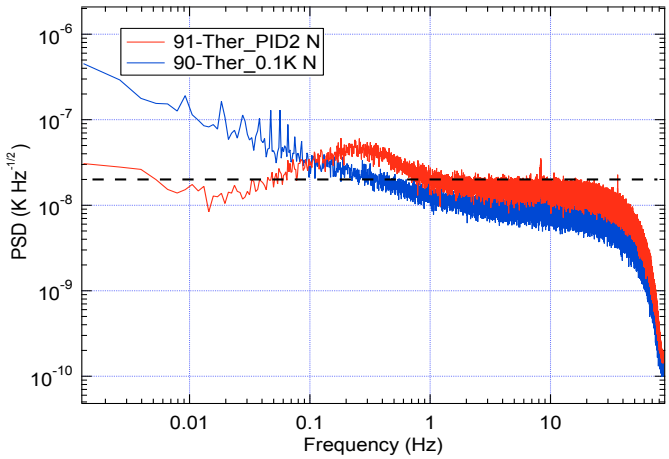

Fig. 27. 100 mK bolometer plate temperature power spectrum during the Saturne PFM calibration. The active PID is controlled by the thermometer 91-Ther PID2 N. The dashed line shows the requirement.

in this range is not a driver of the cooler performance. We end up finally with one parameter adjustable in-flight: the stroke amplitude, and one environment parameter: the pre-cooling provided by the sorption cooler. This last parameter is expected to be close to 17 K at the beginning of the life of the sorption cooler and 17.5 K at the end. A worst case situation is taken to be 18.5 K for which some margin must still be present. The cooler performance was found to be very close to the predictions based on the characterisation during tests at RAL (Rutherford Appleton Laboratory) and the CSL CQM tests. The heat lift performance, measured during the thermal balance test, has shown a 4.5 mW heat lift margin for 3.5 mm stroke amplitude. The heat lift is somewhat higher than the predicted values.

The dilution cooler performed significantly better during the PFM test in Orsay, probably because of the lower precooling temperatures at the different interfaces. The temperature regime reached at CSL could not be achieved in the test facilities used earlier. The improvement is about 6 mK or equivalently 60 nW cooling power. During the TV-TB test, the heat input onto the bolometer plate from micro-vibrations was about 3 to 4 times higher than during the PFM calibration in Orsay (36 nW instead of 10 nW). The in-flight one should be less than 1 nW. The lowest isotope flows were tested at CSL. The best flight operating point in-flight is probably the lowest flow, which can provide 100 mK operations if we take into account the increased flow resulting from the exchange of pressure regulators (19 bars instead of 18 at the entrance of the restrictions) and add an extra margin to the excess liquid production by the 1.6 K JT. It will also increase the lifetime of the HFI survey operations to about 30 months relative to the 15 month baseline.

5.3.2. Dynamical behaviour

The temperature stability requirement for the HFI cryogenic stages was defined by Lamarre et al. (2004). The maximum allowed amplitudes of the temperature fluctuations in the frequency range [10 mHz, 100 Hz] are:

- 4 K horns and filters: 10 μK Hz$^{-0.5}$ (30% emissivity);
- 1.6 K filters: 28 μK Hz$^{-0.5}$ (20% emissivity);
- 0.1 K bolometer plate: 20 nK Hz$^{-0.5}$.

The main driver of these requirements is that the NEP of the associated thermal noises at each stage is equal to one third of the NEP for the total noise in each HFI channel. The HFI active thermal control system is made of various heaters located on the HFI cryogenic stages with a heating power controlled by a PID regulation algorithm implemented in the sensitive thermometer readout system. Stability obtained during the CSL TV-TB test is in agreement or close to the requirements (Figs. 25–27). Because of the very long time needed for stabilization of the 100 mK bolometer plate temperature (tens of hours), its stability at low frequency is expected to be greater in-flight than during the ground-based tests.

6. Conclusion

We have carried out an extensive characterisation and calibration program for the *Planck*-HFI instrument before launch. This provides accurate knowledge about the instrument behaviour and expected performance (see Table 3). For the HFI, the main uncertainties remaining in-flight consist of the true optical background on the detectors, the confirmation of the cryogenic chain performance, and the rate of particle hits. There are therefore few parameters that remain to be adjusted in-flight: the detector bias current, the fine tuning of the cryogenic chain, and the numerical compression. Once the HFI operating point is set, the main goal of the CPV (calibration and performance verification)

Table 3. Determination of main HFI parameters status and references for their values.

	Status and/or determination error	Reference
Beams and far side lobes	computed from front horns and telescope measurements	Maffei et al. (2010), Tauber et al. (2010b)
Spectral bands	0.1 cm^{-1} resolution, $\nu < 400$ GHz: 3% error, $\nu > 400$ GHz: 1% error *final determination within requirement*	Ade et al. (2010)
Polarisation orientation	0.3°/0.6°/2.1° (min/avg/max) for Polarisation Sensistive Bolometers	Rosset et al. (2010)
Cross-polarisation leakage	0.1%/0.2%/2.2% (min/avg/max) for PSB *final determination requires sky data*	
4 K stage emissivity	better than 1%	Sect. 5.1.5
1.6 K stage emissivity	better than 3% for $\nu < 300$ GHz *within requirements to allow correction of remaining systematics coming from thermal stability below*	Sect. 5.1.5
Thermal stability	determined within range [1 mHz, 100 Hz] *flight data required for the final stability determination*	Sect. 5.3.2
Linearity	0.1% determination within requirements	Sect. 5.2.1
Time response	measured to better than 0.1% for 20 detectors *sky data expected for the complete set of detectors*	Sect. 5.2.2
Response	3% determination error *sky data required to provide the absolute calibration*	Sects. 5.1.3, 5.2.1
Total detector noise	explored within range [1 mHz, 100 Hz]	Sect. 5.2.5, Lamarre et al. (2010)
Compatibility	checked to 1% to 3% of noise level *flight data required to provide the ultimate values, including particle hits rate*	Sect. 4.2
Optical crosstalk	down to 60 dB	Sect. 5.1.6
Electrical crosstalk	down to 80 dB *determination within requirement, sky data to reach goal of 80 dB*	Sect. 5.2.4

phase taking place after the launch and before the start of the survey will be to gather all information needed for the reduction of the systematic effects. The balance we have achieved between the pre-launch and the in-flight calibration strategies should allow us to maximize the effective duration of the survey, hence the scientific return of the *Planck* mission.

Acknowledgements. The authors would like to express their gratitude to the CSL team for its contributions and support to the *Planck* cryogenic test campaigns.

References

Ade, P. A. R., Savini, G., Sudiwala, R., et al. 2010, A&A, 520, A11
Aumont, J., Conversi, L., Thum, C., et al. 2010, A&A, 514, A70
Benoît, A., Ade, P. A. R., & Amblard, A. 2002, Astrop. Phys., 17-2, 101
Bernard, J.-P., Ade, P. A. R., De Bernardis, P., et al. 2007, EAS Publications Ser., 23, 189
Bersanelli, M., Mandolesi, N., Butler, R. C., et al. 2010, A&A, 520, A4
Fixsen, D. J., Cheng, E. S., Cottingham, D. A., et al. 1994, ApJ, 420-2, 457
Henrot-Versillé, S., Cizeron, R., & Couchot, F. 2009, Infrared Phys. & Techn., 52, 159
Holmes, W. A., Bock, J. J., Crill, B. P., et al. 2008, Appl. Opt., 47, 5996
Huffenberger, K. M., Crill, B. P., Lange, A. E., Górski, K. M., & Lawrence, C. R. 2010, A&A, 510, A58
Lamarre, J.-M., Puget, J.-L., Bouchet, F., et al. 2003, New Astron. Rev., 47, 1017
Lamarre, J.-M., Puget, J.-L., Ade, P. A. R., et al. 2010, A&A, 520, A9
Maffei, B., et al. 2000, Int. J. IRMMW, 21, (12) 2023
Maffei, B., Noviello, F., Murphy, J. A., et al. 2010, A&A, 520, A12
Masi, S., Ade, P. A. R., Bock, J. J., et al. 2006, A&A, 458, 687
Mather, J. C., Fixsen, D. J., Shafer, R. A., et al. 1999, ApJ, 512, 511
Mennella, A., et al. 2010, A&A, 520, A5
Page, L., Jackson, C., Barnes, C., et al. 2003, ApJ, 585, 566
Pajot, F., Lamarre, J.-M., & Puget, J.-L. 2008, CA-PH412-600824-IAS-Issue 02 Rev 01
Pajot, F., Stepnik, B., Lamarre, J.-M., et al. 2006, A&A, 447, 769
Piat, M., Lagache, G., Bernard, J.-P., et al. 2002, A&A, 393, 359
Rosset, C., Tristram, M., Ponthieu, N., et al. 2010, A&A, 520, A13
Tauber, J. A., Mandolesi, N., Puget, J.-L., et al. 2010a, A&A, 520, A1
Tauber, J. A., Norgaard-Nielsen, H.-U., Ade, P. A. R., et al. 2010b, A&A, 520, A2
Torre, J.-P., & Chanin, G. 1985, Rev. Scient. Inst., 26, 328
Vigroux, L., Cesarsky, C., Boulade, O., et al. 1993, Proc. SPIE, 1946, 281

[1] Institut d'Astrophysique Spatiale, Bât. 121, Université Paris Sud-11, 91405 Orsay, France
e-mail: francois.pajot@ias.u-psud.fr
[2] Astronomy and Instrumentation Group, Cardiff University, Cardiff, Wales, UK
[3] Laboratoire de l'Accélérateur Linéaire, Université Paris Sud-11, 91405 Orsay, France
[4] Laboratoire Astroparticule et Cosmologie (APC), UMR 7164, CNRS & Université Paris Diderot – Paris 7, 10 rue A. Domon et L. Duquet, 75205 Paris Cedex 13, France
[5] Institut Néel, CNRS/UJF, 25 rue des Martyrs, BP 166, 38042 Grenoble Cedex 9, France
[6] LERMA, CNRS, Observatoire de Paris, 61 Avenue de l'Observatoire, 75014 Paris, France
[7] Department of Physics, California Institute of Technology, Mail code:59-33, Pasadena, CA 91125, USA
[8] Jet Propulsion Laboratory, California Institute of Technology, 4800 Oak Grove Drive, Pasadena, CA 91109, USA
[9] Gruppo di Cosmologia Sperimentale, Dipart. di Fisica, Univ. La Sapienza, P. A. Moro 2, 00185 Roma, Italy
[10] Institut d'Astrophysique de Paris, UMR7095, CNRS and Université Pierre & Marie Curie-Paris-6, 98 bis boulevard Arago, 75014 Paris, France
[11] Laboratoire d'Astrophysique, Obs. de Grenoble, BP 53, 38041 Grenoble Cedex 9, France
[12] Centre d'Etude Spatiale des Rayonnements, CNRS, 9 Avenue du Colonel Roche, BP 4346, 31028 Toulouse, France
[13] Princeton University, Department of Physics, Joseph Henry Laboratory, USA
[14] LPSC, Université Joseph Fourier Grenoble I, CNRS/IN2P3, Institut National Polytechnique de Grenoble, 53 Avenue des Martyrs, 38026 Grenoble Cedex, France
[15] CNES, Centre spatial de Toulouse, 18 avenue Edouard Belin, 31401 Toulouse Cedex 9, France
[16] The University of Manchester, School of Physics and Astronomy, Alan Turing Building, Manchester M13 9PL, UK
[17] Optical Science Laboratory, University College London, Gower Street, WC1E 6BT London, UK
[18] CEA-CE Saclay, DAPNIA, Service de Physique des Particules, Bât. 141, 91191 Gif-sur-Yvette Cedex, France